Hindawi
Journal of Nanomaterials
Volume 2017, Article ID 6759853, 9 pages
https://doi.org/10.1155/2017/6759853

Research Article

Synthesis and Characterization of the Optical Properties of Pt-TiO_2 Nanotubes

Zhuwu Jiang,[1] Jingling Li,[1] Wei Liao,[1] Gongduan Fan,[2] Hualiang Yu,[3] Lihong Chen,[1] and Zhaoyue Su[2]

[1]*College of Ecological Environment and Urban Construction, Fujian University of Technology, Fuzhou 350108, China*
[2]*College of Civil Engineering, Fuzhou University, Fuzhou 350116, China*
[3]*Department of Physics and Electronics, Minjiang University, Fuzhou 350108, China*

Correspondence should be addressed to Zhuwu Jiang; jiangzhuwu@126.com and Gongduan Fan; fgdfz@fzu.edu.cn

Received 13 January 2017; Revised 25 March 2017; Accepted 28 March 2017; Published 13 August 2017

Academic Editor: Stefano Bellucci

Composite Pt-doped TiO_2 nanotubes (Pt-TNTs) were synthesized via alkaline fusion-hydrothermal method (AFHM) under ambient atmosphere pressure. Further systematic characterization of Pt-TNTs was performed by using XPS, surface photovoltage spectroscopy (SPS), electric field-induced surface photovoltage spectroscopy (FISPS), UV-Vis diffuse reflectance spectrophotometry (UV-Vis), TEM, and XRD. XPS spectrum showed double peaks which accounted for the presence of platinum dioxide and platinum oxide (PtO_2 and PtO, $PtO_x^{\delta+}$). Composition analysis showed that the particulate matters on surface of Pt-TNTs were composed of $PtO_x^{\delta+}$ and TiO_2. The results of SPS and FISPS demonstrated that the bound exciton showed sub-band gap transition characteristics with the asymmetric changes of photoelectric property corresponding to changes in polarity and strength of the external electric field. Furthermore, the influence of the changed microstructure morphology of Pt-doped TNTs on both the photovoltage spectroscopy and the lifetime of photogenerated carriers which occurred at the interfaces of Pt-TNTs was observed. Result of XRD indicated that a mixture of anatase and rutile phases prevailed in Pt-TNTs. Contact potential barriers consisting of $PtO_x^{\delta+}$, anatase, rutile, and $PtO_x^{\delta+}$ are presumed to form upon $PtO_x^{\delta+}$ particle that deposited on the surface of Pt-TNTs.

1. Introduction

TiO_2, as a kind of semiconductor material, is well known for its stability, being ecofriendly, and other interesting physical and chemical properties. It is widely used in wastewater treatment and catalyst process [1, 2]. Because of its wider band gap (3.2 eV), only the ultraviolet portion (<380 nm) can be absorbed effectively by TiO_2, hindering its practical application as a photocatalyst [3]. Many researches have been performed to extend its absorption spectrum to the visible range (400 nm–700 nm). Some of the strategies to improve its light quanta yield are to modify these nanomaterials with noble metals [4–6] and nonmetallic elements [7, 8] or synthesize composite semiconductors [9–11]. With these approaches, one could achieve efficient charge separation upon photoexcitation and there are several reports highlighting the effect of modifying TiO_2 nanomaterials with a series of noble metals such as Ag and Pt [12, 13].

There are various publications regarding the lifetime of the carriers and their migration mechanism on the surface of TiO_2 nanomaterials modified by noble metal. For example, elemental doping can result in lattice defects, changing the microstructure of TiO_2 nanoparticles. The modification of the microstructure can enhance the separation property of electrons and holes effectively. Gerischer and Heller [14] showed that the lattice defects could modulate the Fermi energy level of TiO_2 and increase the surface energy barriers, reducing the recombination rate of the photogenerated electrons and holes on the surface of TiO_2.

Moreover, the work function of noble metals is generally larger than TiO_2 [15–19]. Therefore, the combination of their different work functions forms a contact barrier that also influences the migration and lifetime of the photogenerated carriers. The charge carriers' lifetime will be prolonged if the neutralization is weakened. Since the discovery of carbon

nanotubes in 1991 [20], nanotube materials has gradually become a research hotspot around the world [21]. Because of their sensitivity to humidity, photoluminescence, and other physicochemical properties, TiO_2 nanotubes (TNTs), as sensors [22, 23], hydrogen storage devices [24, 25], and photocatalysts [26], play an important role in the new century. Compared to particles or agglomerate forms, TNTs are expected to further expand their applications as sensors, hydrogen storage materials, solar energy cells, and photocatalysts, due to their larger surface area, greater length-diameter ratio (aspect ratio), and nanometer-scale hollow passageway [23, 27, 28].

The speech delivered by Brattain and Bardeen opened a new phase of surface photovoltaic research in the late 1940s and early 1950s [29]. Johnson and Goodman [30, 31] measured the lifespan of carriers utilizing SPV (Surface Photovoltage Spectroscopy) and developed a theoretical model to determine minority carriers' diffusion length, leading to the foundation of silicon solar cells in the 1960s. Brillson [32] sorted out a clear relationship between the chemical microstructures and electronic properties on all sorts of surfaces of different semiconductors. Lu et al. carried out comprehensive study to reveal the characteristics of surface photovoltages in detail [13, 33, 34].

Currently, noble metal-doped TNTs are mainly synthesized by sol-gel, chemical deposition, or impregnation process [19, 35, 36]. Hydrothermal method is a simple and economical way to synthesize TNTs to achieve a high yield. However, due to its nature of pressurized process, it is not suitable to be widely applied in industrial production. Therefore, in this work, Pt-doped TiO_2 nanotubes were synthesized via hydrothermal methods under ambient atmosphere pressure. This method is cost-efficient and simple to operate and has the potential for industrial production. In order to comprehensively investigate the surface features of the microstructure morphology of Pt-TNTs, based on our previous reported works [15, 37], Pt was chosen as the doped material, and the alkali fusion-hydrothermal method (AFHM) was conducted to synthesize the Pt-TNTs under atmospheric pressure. A systematic investigation of the optoelectrical properties of the nanocomposites was also carried out using XPS, SPS, FISPS, UV-Vis, TEM, EDX (Energy Dispersive X-Ray Spectroscopy), and XRD.

2. Methods and Materials

2.1. Materials Characterization Methods. The experimental instruments included TEM (Model JEM-2010), XRD (BRUKER, D8 ADVANCE), Multielectron spectrometer (ESCALAB 250), and UV-Vis (CARY 500, Varian Company). Raman spectroscopy was performed using Renishaw In-Via Raman microscope in an excitation line of 785 nm produced by double Nd: YAG laser. SPS and FISPS were carried out in a device consisting of a source of monochromatic light, a lock-in amplifier with a light chopper (SR540), and a photovoltaic cell [33]. The monochromator and the lock-in amplifier were interfaced to a computer, a 500 W xenon lamp and a grating monochromator provide monochromatic light, and the construction of the photovoltaic cell was a sandwich-like structure of ITO-sample-ITO.

2.2. Synthesis of Pt-TNTs with AFHM. Titanium dioxide (TiO_2, Tianjin Fu Chen Chemical Reagents Factory), potassium platinic chloride (K_3PtCl_6, Shanghai SSS Reagent Co., Ltd.), and sodium hydroxide (NaOH, Shanghai Yijiu Chemical Reagent Co., Ltd.) used in this study were of analytical grade.

TiO_2 raw materials (TR) and NaOH were separately put into three alundum crucibles each with a volume of 50 ml according to a ratio of 1 : 8. The three alundum crucibles were labeled as Pt-TNTs1, Pt-TNTs3, and Pt-TNTs5. 0.24 g, 0.75 g, and 1.25 g of K_3PtCl_6 were sequentially added and fully mixed with TR and NaOH to reach Pt ions concentration of 1.0, 3.0, and 5.0 wt% (labeled as Pt-TNTs1, Pt-TNTs3, and Pt-TNTs5), respectively. The abovementioned alundum crucibles were then placed in a muffle furnace to be melted at 650°C for 30 minutes. The crucibles with the melted solid were removed from the furnace to cool down to ambient temperature, and the melted solids were then put into three plastic beakers. A certain amount of distilled water was added, maintaining NaOH concentration no less than 10 M. The plastic beakers with the deposition mixtures were then put into the oven at 110°C for 72 h. After cooling down to ambient temperature, the deposition mixtures involving Pt-TNTs were washed with tap water, distilled water, 2% HNO_3 solution, and distilled water, respectively. The deposition mixtures were then transferred to three glass beakers to finish the drying step. Thereafter, the glass beakers with Pt-TNTs (labeled as Pt-TNTs1, Pt-TNTs3, and Pt-TNTs5) were put into the muffle furnace and heated to 550°C at an increasing rate of 5°C/min and then sustained for 2 h. Pt-TNTs1, Pt-TNTs3, and Pt-TNTs5 had to be ground after cooling down to ambient temperature.

The conversion rate of raw titania powder into titania nanotubes was about 90% for nanotubes with length between 100 nm and 200 nm, indicating a good potential for industrial production.

3. Results and Discussion

3.1. XPS of Pt-TNTs. The Pt-TNTs were found to generate platinum oxide $PtO_x^{\delta+}$ (PtO and PtO_2, with δ^+ in both +2 and +4 states while x = 1 and 2, resp.) [38, 39] after calcination at 550°C. As shown in Figure 1(a), with respect to Ti, the electron binding energies of $Ti2p_{3/2}$ and $Ti2p_{1/2}$ were located at 458.72 eV and 464.38 eV, respectively. The difference between the peaks of $Ti2p_{3/2}$ and $Ti2p_{1/2}$ with the electron binding energy of 5.66 eV indicated that Ti^{4+} existed in the primary state. No reduction in the valence state of titanium was observed in the Pt-TNTs. As can be seen from Figure 1(b), the peak corresponding to O1s was observed at 530.15 eV. As shown in Figure 1(c), it could be deduced that 3.03% of Pt atoms were on the surface of Pt-TNTs. XPS of the Pt4f spectrum could be fitted into two groups of double peaks which resulted from the form of platinum oxide $PtO_x^{\delta+}$ (as PtO and PtO_2, at 72.03 eV and 74.33 eV for $Pt4f_{7/2}$, resp.) at high binding energy as well as metallic Pt at low binding energy (Pt, at 71.1 eV for $Pt4f_{7/2}$). A peak shift of 2.55 eV observed for $Pt4f_{5/2}$ from the lower binding energy (75.00 eV) to a higher binding (77.55 eV) energy also

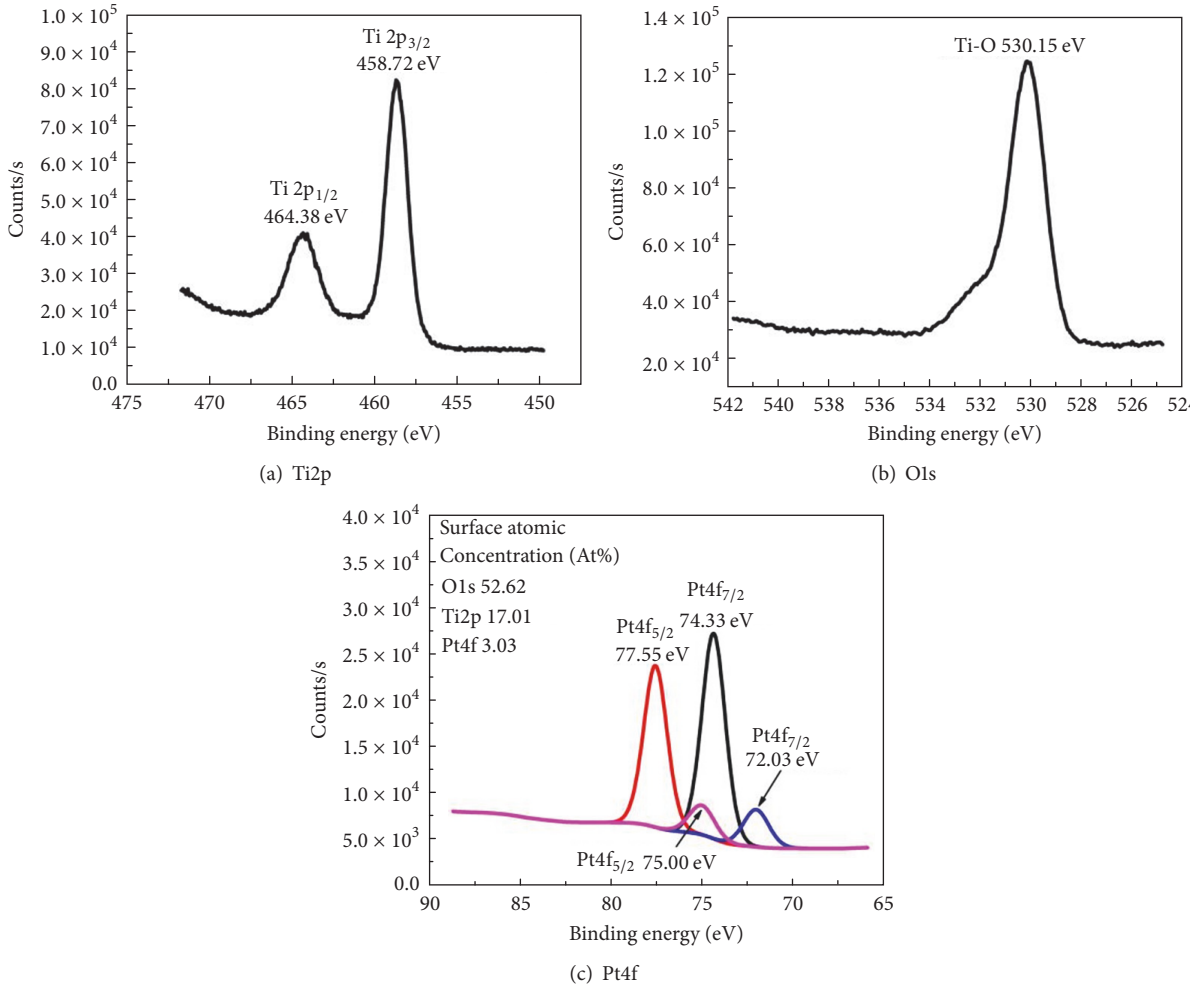

Figure 1: XPS survey spectrum of Pt-TNTs3.

indicated the oxidization process from Pt^{2+} to Pt^{4+}. Platinum oxides would result in lattice defects on the surface of Pt-TNTs, forming trapping sites for photogenerated electrons [19, 38, 40].

3.2. XRD of Pt-TNTs. The diffraction pattern of Pt-TNTs is shown in Figure 2. The peaks of XRD for TR existed only in the anatase phase (JCPDS Card Number 21-1272), while the peaks of both anatase and rutile were present in Pt-doped TNTs (JCPDS Card 21-1276). There was no fundamental change in the crystal type of Pt-TNTs due to Pt doping. The change in microstructure and morphology of Pt-TNTs was caused by the process of AFHM under ambient atmosphere pressure. There was no signature peak of Pt diffraction in the diffraction pattern, which resulted from the platinum oxide, $PtO_x^{\delta+}$.

3.3. TEM of Pt-TNTs. TEM images of the as-synthesized Pt-TNTs are shown in Figure 3. The formation mechanism for Pt-TNTs is similar to that reported in the literature [41]; that is, the AFHM and alkali solution under ambient atmosphere pressure will distort the octahedral crystal structure of TiO_2 nanoparticles. Titanium atoms in octahedral structure [TiO_6] form Ti-O bonds, growing along the [100] direction and flanking along the [010] direction. Particles on the surfaces of nanotube are recognized as platinum oxide $PtO_x^{\delta+}$ and TiO_2 [39]. During sintering of the Pt-TNTs at higher temperatures such as 650°C in the synthesis process, $PtO_x^{\delta+}$ particles spread out over the Pt-TNTs surfaces and then formed agglomerated particles. As shown in TEM images of Pt-TNTs, Pt nanoparticles adhered to the surfaces of TNTs.

From the EDX analysis that is shown in Figure 4, it can be deduced that the TNTs were comprised of Ti, Pt, Na, and other elements.

3.4. SPS and FISPS of Pt-TNTs. In order to further investigate the photoelectric properties of Pt-TNTs, surface photovoltage spectra (SPS) and electric field induced surface photovoltage spectroscopy (FISPS) of Pt-TNTs were analyzed. The results of SPS revealed the presence of an electronic interaction in Pt-TNTs (Figures 5 and 6). SPS response intensity of TR and Pt-TNTs with different doping amount showed significant photovoltage signals in the ultraviolet region. The TNTs doped with Pt ions at a concentration of 1%, 3%,

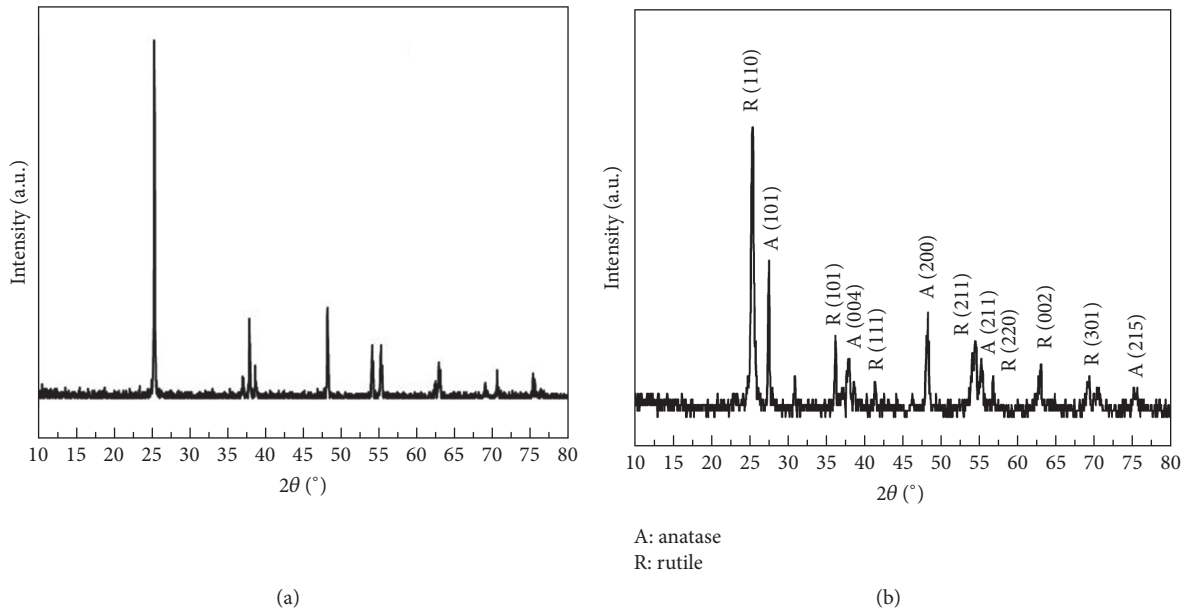

Figure 2: XRD patterns of TiO_2 nano materials. (a) shows curves of TR. (b) Pt-TNTs3 via AFHM.

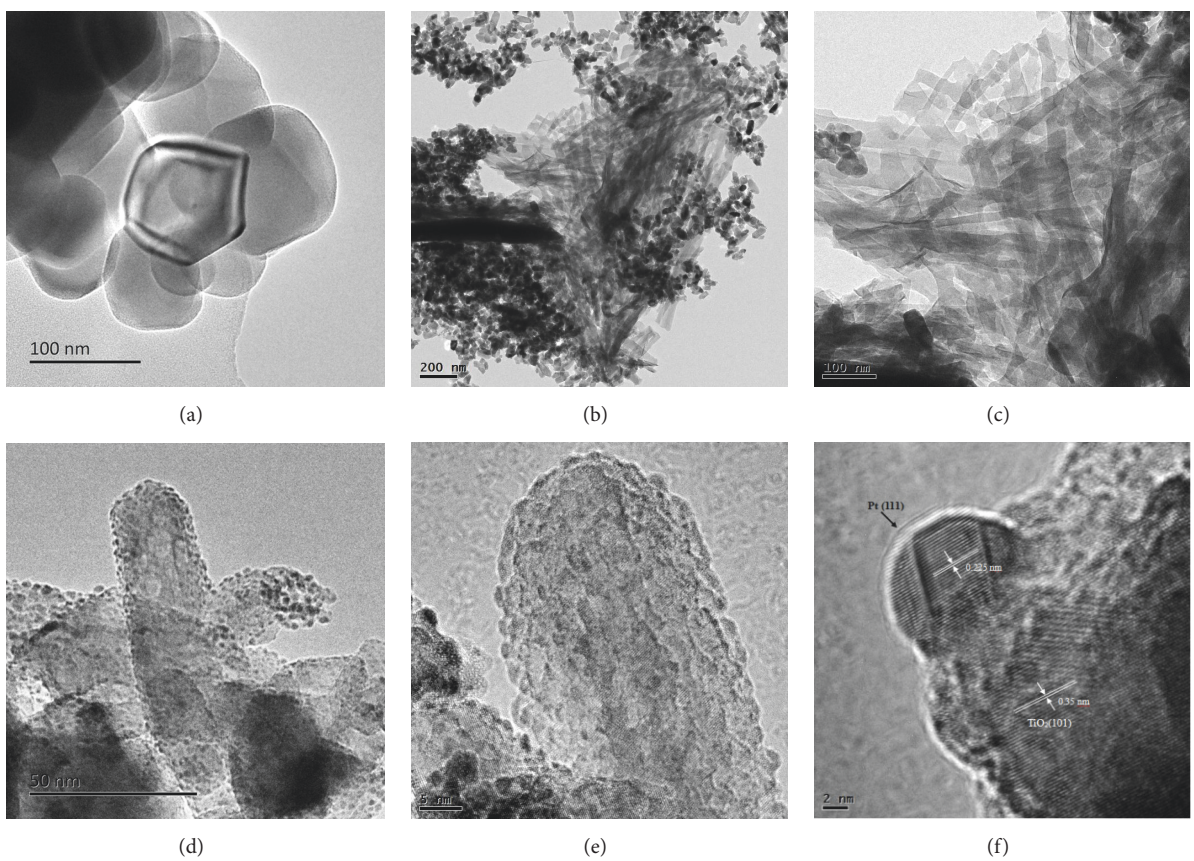

Figure 3: TEM images of composite Pt-TNTs of (a) TR, ((b) and (c)) Pt-TNTs3; ((d), (e), and (f)) Pt-TNTs5.

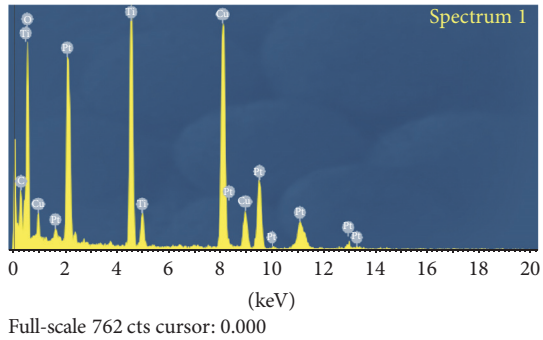

Figure 4: EDX analysis showing the composition of Pt-TNTs.

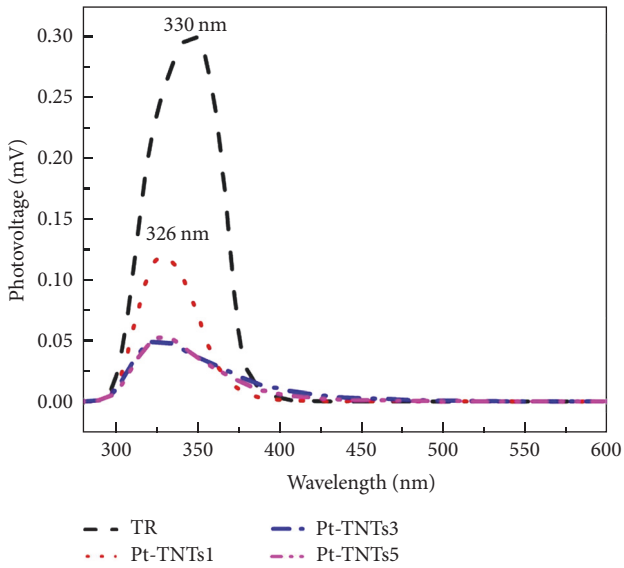

Figure 5: SPS of TR and Pt-TNTs1, Pt-TNTs3, and Pt-TNTs5.

and 5% (wt) were denoted as Pt-TNTs1, Pt-TNTs3, and Pt-TNTs5, respectively. The wavelengths of the TR and Pt-TNTs corresponding to the maximum SPS value were 339.52 nm and 328.21 nm, respectively. As can be seen from Figure 5, Pt-TNTs showed a photovoltaic response with peaks shifting from 339.52 nm (for Pt-TNTs0) to 328.21 nm (for Pt-TNTs5).

However, a mismatch between the photovoltaic response and absorption was observed as there was some blue-shift in the photovoltaic response for the Pt-TNTs (from 330 nm for TR to 326 nm for Pt-TNTs). These results implied that the formation efficiency of photogenerated electron-hole pairs was much lower than that of photon absorption when Pt-TNTs were motivated by the lower wavelength light, resulting from the different electronic transitions among SPS, FISPS, and UV-Vis absorption spectra [42]. From the perspective of photovoltage response for the Pt-TNTs which was lower than that of pristine TNTs, it seemed fair to suggest that the deposited PtO and PtO_2 nanoparticles (not Pt metal) acted as electron traps on the surface of Pt-TNTs.

According to Figure 6, it was observed that a gradual increase in Pt doping (0 wt%, 1 wt%, 3 wt%, and 5 wt%) was accompanied by a corresponding change in the SPS of the Pt-TNTs. The dopant concentration would reduce the quantum efficiency, as they acted as recombination sites for electrons and holes. The doping amount has a considerable impact on the generation and recombination of electron-hole pairs in the Pt-TNTs. Differences were found among the impurity energy levels formed by doping on the surface of Pt-TNTs as well as between the impurity levels and the top of the valence band. The impurity levels served as new shallow bands of electron acceptors, which narrowed the band gap and enhanced migration of the carriers, resulting in a subsequent reduction of recombination between photogenerated electrons and holes [43].

FISPS of TR and Pt-TNTs with different dopant concentration are shown in Figure 6. A band-band transition induced by the external electric field for TR and Pt-TNTs (Pt ions added at an amount of 0 wt%, 1 wt%, 3 wt%, and 5 wt%) are shown in Figures 6(a), 6(b), 6(c), and 6(d), respectively. The photovoltaic response increased rapidly with the addition of positive electricity field and decreased with the addition of negative electricity field. Furthermore, the change in photovoltaic response was not symmetric based on the variation of field intensity [44, 45]. The quantum confinement effect of photogenerated charges could be attributed to the fact that the binding force of confined energy levels (or the surface states for the photogenerated electrons) was greater than that for the photogenerated holes, which was a characteristic of the bound excitons transition. The asymmetric response resulted from the confined energy levels of the excitons bound by the external electric field.

3.5. UV-Vis Diffuse Reflectance Spectrophotometry. The band gap energy of Pt-TNTs is calculated according to the Kubelka-Munk equation [3]. The band gaps of TR and Pt-TNTs were 3.20 eV and 2.92 eV, respectively (Figure 7). Pt-TNTs exhibited two kinds of characteristic light absorption edges in the UV-Vis spectra. One was in the UV region that was attributable to the band gap of raw materials TiO_2, resulting from the photogenerated electronics transition from O^{2-} antibonding orbital to Ti^{4+} minimum empty orbital. Corresponding to photogenerated electrons band-band intrinsic transition, Pt-TNTs was in the visible spectra from 387 nm to 424 nm, in line with the impurity energy level due to Pt doping. The absorption edges of TR and TNTs were located at about 387 nm (corresponding to 3.20 eV) and 424 nm (2.92 eV), respectively. The redshift could be due to the generation of new levels of impurities in the band gap of Pt-TNTs, caused by Pt doping. These new levels of impurities led to narrowing of the band gap of Pt-TNTs and were regarded as deep levels in the bound exciton transition.

3.6. Contact Potential Barriers on the Interfaces of $PtO_x^{\delta+}$, Anatase, and Rutile. The difference of contact potential barriers arose from the contacts among $PtO_x^{\delta+}$, anatase, and rutile and the difference of their work function values (Figure 8). Contact potential barriers were presumed to form upon $PtO_x^{\delta+}$ particle deposition on the surface of Pt-TNTs. The work function values of TR were estimated to be 4.72 eV via Kelvin probe technique [15]. The work function values

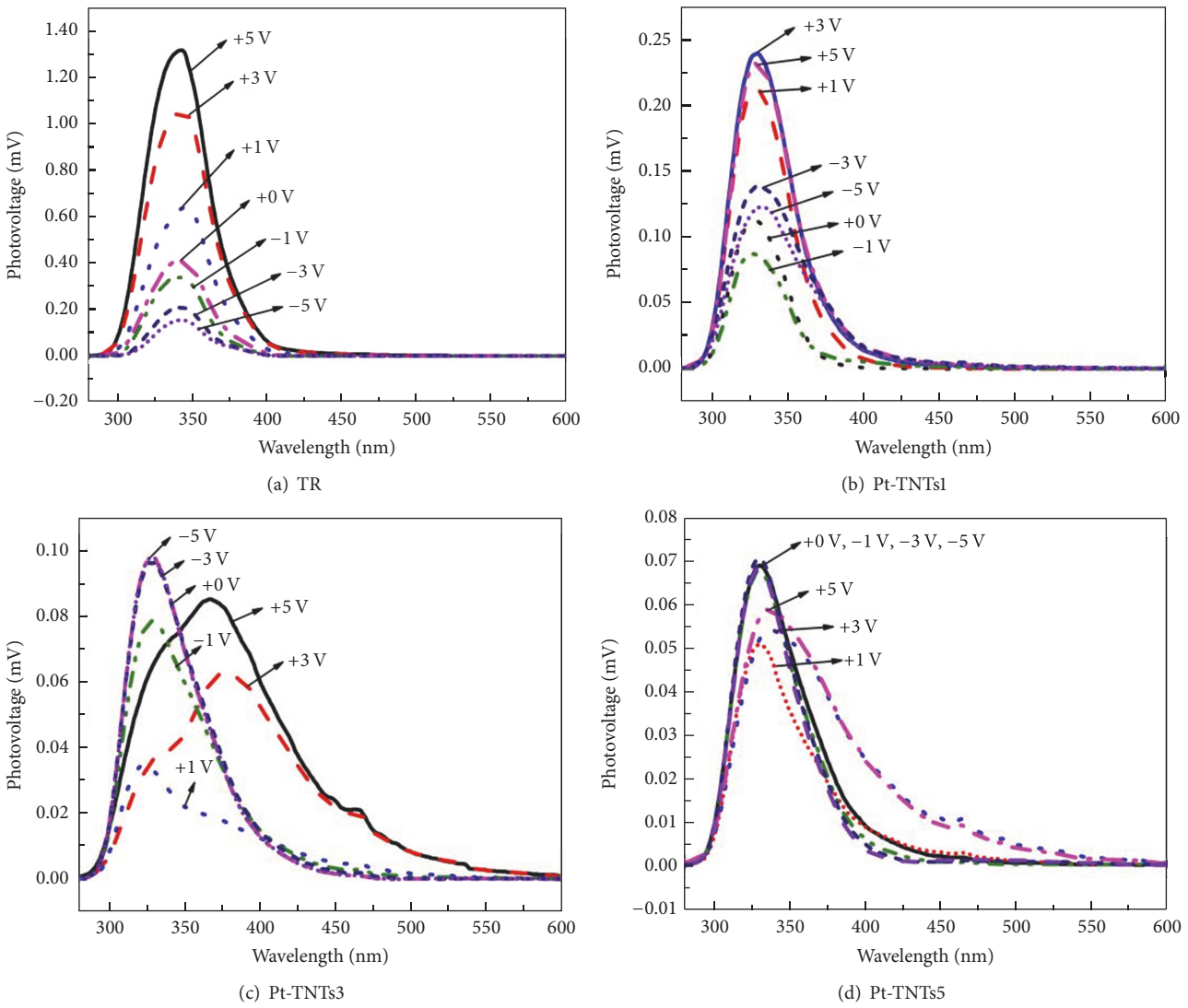

Figure 6: FISPS of TR and Pt-TNTs1, Pt-TNTs3, and Pt-TNTs5.

of titanium and Pt were found to be 4.45 eV and 5.65 eV, respectively [46]. The descending order of the surface work functions was Pt, anatase TiO_2, mixed-phase, and rutile TiO_2 [47–49].

Based on previously reported surface work functions values for $PtO_x^{\delta+}$, anatase, and rutile, we could infer that E_F of $PtO_x^{\delta+}$ was the highest and rutile was the lowest and mixed-phase fell in between. The Fermi level (E_F) of $PtO_x^{\delta+}$ was higher than that of anatase and rutile TiO_2, while E_F of anatase TiO_2 was higher than that of rutile TiO_2. Therefore, there were three built-in electric fields (Figure 8(a)) which formed the contact potential barriers coming from $PtO_x^{\delta+}$-anatase, anatase-rutile, and $PtO_x^{\delta+}$-rutile. They were located above the valence band of TiO_2 (as shown in Figure 8(b)).

Therefore, the photoelectrons had a higher probability to transfer from rutile to anatase and from mixed-phase to $PtO_x^{\delta+}$ when the nanoparticles of $PtO_x^{\delta+}$, anatase, and rutile with different phases came to contact. In other words, there were three possible ways of transferring the in-contact photoelectrons under different phases. The first pathway was to transfer from rutile to $PtO_x^{\delta+}$, the second pathway was to transfer from rutile to $PtO_x^{\delta+}$, and the third pathway was to transfer from rutile to anatase. It is important to understand that the three mechanisms could occur simultaneously. Photogenerated electron-hole pairs were thus effectively separated by the three electric fields. Specifically, excessive nonequilibrium photo holes would concentrate in the region of possessing lower work function (e.g., in anatase and rutile), whereas excessive nonequilibrium photoelectrons would gather within the $PtO_x^{\delta+}$ particles. Contact potential barriers significantly hindered the recombination of photoelectrons and photo holes, thereby enhancing the photocatalytic efficiency.

4. Conclusions

Composite Pt-TNTs were synthesized via AFHM under ambient atmosphere pressure with their photoelectrical and

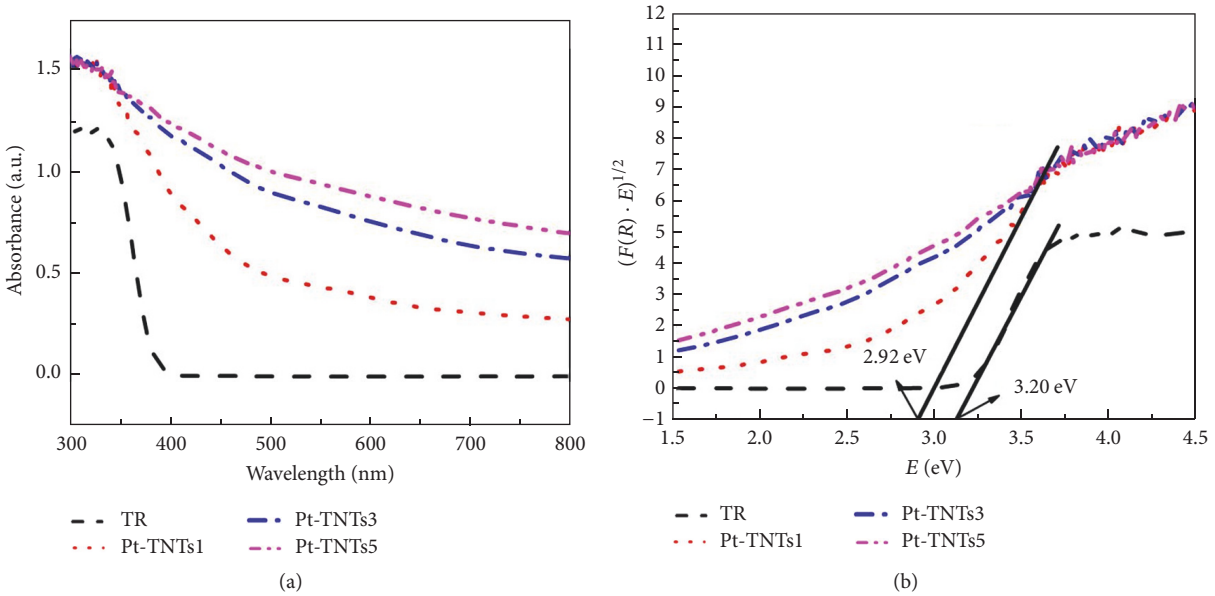

FIGURE 7: UV-vis diffuse reflectance spectra of TR and Pt-TNTs1, Pt-TNTs3, and Pt-TNTs5.

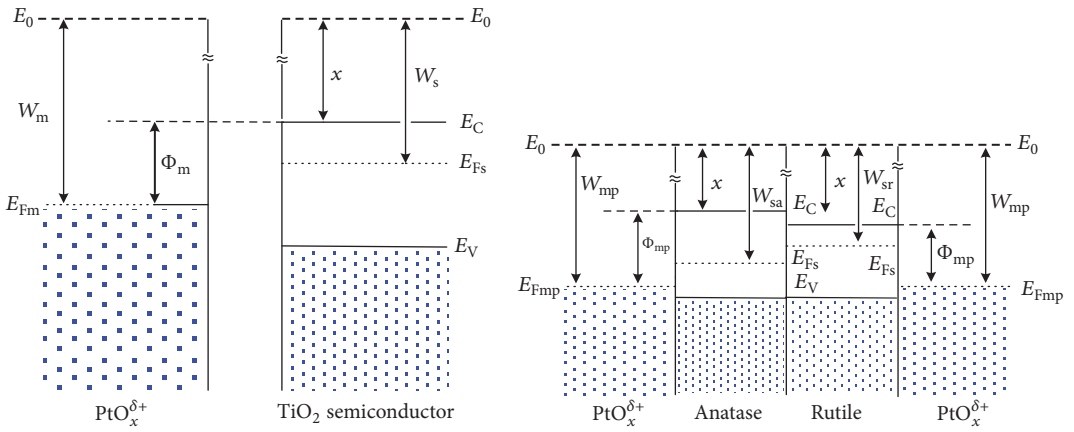

(a) $PtO_x^{\delta+}$ and TiO_2 semiconductor before being in contact

(b) $PtO_x^{\delta+}$ being in contact with rutile and anatase, respectively

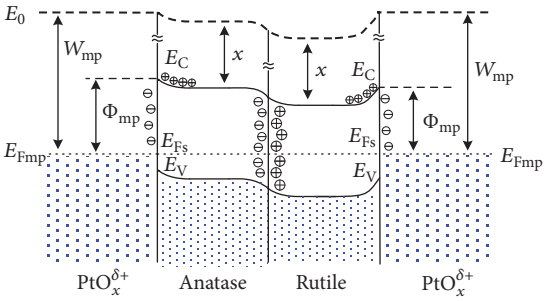

(c) $PtO_x^{\delta+}$ being in contact with rutile and anatase, respectively

FIGURE 8: Schematic band diagrams among $PtO_x^{\delta+}$, anatase, and rutile interface of Pt-TNTs.

optical properties characterized by XPS, TEM, SPS, and FISPS. The depositions of particulate matters on Pt-TNTs surface were platinum oxide ($PtO_x^{\delta+}$) and mixed-phase titanium oxide (rutile and anatase TiO_2). It can be concluded that contact potential barriers consisting of $PtO_x^{\delta+}$-anatase, anatase-rutile, and rutile-$PtO_x^{\delta+}$ are present which arise from the difference in the work function of different phases.

Conflicts of Interest

The authors declare that they have no conflicts of interest.

Acknowledgments

The authors gratefully acknowledge the financial support from the major S&T projects of university-industry collaboration in Fujian (2016H6003), Scientific Research Foundation of Fujian University of Technology (GY-Z160042), Fujian Provincial Natural Science Fund (2017J01770), and Scientific Research Foundation of Fuzhou (2016-G-71). They are also grateful to Ms. SHI Ronghui, Ms. CHEN Jun from Fujian University of Technology, and Ms. Zhang Yinfei Ellen from the University of Hong Kong.

References

[1] Z. Ding, G. Q. Lu, and P. F. Greenlield, "Role of the crystallite phase of TiO_2 in heterogeneous photocatalysis for phenol oxidation in water," *The Journal of Physical Chemistry B*, vol. 104, pp. 4815–4820, 2000.

[2] H. Einaga, M. Harada, S. Futamura, and T. Ibusukiet, "Generation of active sites for CO photooxidation on TiO_2 by platinum deposition," *The Journal of Physical Chemistry B*, vol. 107, pp. 9290–9297, 2003.

[3] A. Zielińska-Jurek, I. Wysocka, M. Janczarek, W. Stampor, and J. Hupka, "Preparation and characterization of Pt-N/TiO2 photocatalysts and their efficiency in degradation of recalcitrant chemicals," *Separation and Purification Technology*, vol. 156, pp. 369–378, 2015.

[4] H. Li, Z. Bian, J. Zhu, Y. Huo, H. Li, and Y. Lu, "Mesoporous Au/TiO_2 nanocomposites with enhanced photocatalytic activity," *Journal of the American Chemical Society*, vol. 129, no. 15, pp. 4538-4539, 2007.

[5] W.-W. Yu, Q.-H. Zhang, G.-Y. Shi, Y.-G. Li, and H.-Z. Wang, "Preparation of pt-loaded TiO2 nanotubes/nanocrystals composite photocatalysts and their photocatalytic properties," *Wuji Cailiao Xuebao/Journal of Inorganic Materials*, vol. 26, no. 7, pp. 747–752, 2011.

[6] W. Choi, A. Termin, and M. R. Hoffmann, "The role metal ion dopants in quantunsided TiO_2: corre-lation between photoreactivity and charge carrier recombination dynamics," *Journal of Physical Chemistry*, vol. 98, no. 51, pp. 13669–13679, 1994.

[7] R. Asahi, T. Morikawa, T. Ohwaki, K. Aoki, and Y. Taga, "Visible-light photocatalysis in nitrogen-doped titanium oxides," *Science*, vol. 293, no. 5528, pp. 269–271, 2001.

[8] Y. Sakatani, H. Ando, K. Okusako et al., "Metal ion and N co-doped TiO_2 as a visible-light photocatalyst," *Journal of Materials Research*, vol. 19, no. 7, pp. 2100–2108, 2004.

[9] Z. Liu, D. D. Sun, P. Guo, and J. O. Leckie, "An efficient bicomponent TiO_2/SnO_2 nanofiber photocatalyst fabricated by electrospinning with a side-by-side dual spinneret method," *Nano Letters*, vol. 7, no. 4, pp. 1081–1085, 2007.

[10] S. V. Chong, N. Suresh, J. Xia, N. Al-Salim, and H. Idriss, "TiO_2 nanobelts/CdSSe quantum dots nanocomposite," *The Journal of Physical Chemistry C*, vol. 111, no. 28, pp. 10389–10393, 2007.

[11] K. R. Copidas, M. Bohorgaez, and P. V. Kamat, "Photophysical and photochemical aspect of coupled semiconductors: charge-transfer processes in colloidal CdS-TiO_2 and CdS-AgI system," *Journal of Physical Chemistry*, vol. 94, no. 16, pp. 6435–6440, 1990.

[12] J. Lagowski, P. Edelman, M. Dexter, and W. Henley, "Noncontact mapping of heavy metal contamination for silicon IC fabrication," *Semiconductor Science and Technology*, vol. 7, no. 1 A, article no. 036, pp. A185–A192, 1992.

[13] Y. Lu, Y. Lin, D. Wang, L. Wang, T. Xie, and T. Jiang, "Surface charge transfer properties of high-performance Ag-decorated ZnO photocatalysts," *Journal of Physics D: Applied Physics*, vol. 44, no. 31, Article ID 315502, 2011.

[14] H. Gerischer and A. Heller, "The role of oxygen in photooxidation of organic molecules on semiconductor particles," *The Journal of Physical Chemistry*, vol. 95, no. 13, pp. 5261–5267, 1991.

[15] J. L. Li, W. Z. Chen, H. L. Yu et al., "Contact potential barriers and characterization of Ag-doped composite TiO_2 nano materials," *Journal of Physics & Chemistry of Solids*, vol. 75, no. 4, pp. 505–511, 2014.

[16] K. Onda, B. Li, and H. Petek, "Two-photon photoemission spectroscopy of TiO2(110) surfaces modified by defects and O2 or H2O adsorbates," *Physical Review B - Condensed Matter and Materials Physics*, vol. 70, no. 4, Article ID 045415, pp. 1–45415, 2004.

[17] G. Xiong, R. Shao, T. C. Droubay et al., "Photoemission electron microscopy of TiO2 anatase films embedded with rutile nanocrystals," *Advanced Functional Materials*, vol. 17, no. 13, pp. 2133–2138, 2007.

[18] G. Liu, W. Jaegermann, J. He, V. Sundström, and L. Sun, "XPS and UPS characterization of the TiO2/ZnPcGly heterointerface: Alignment of energy levels," *Journal of Physical Chemistry B*, vol. 106, no. 23, pp. 5814–5819, 2002.

[19] L. Jiang, W. Zhu, C. Wang et al., "Preparation of hollow Ag/Pt heterostructures on TiO_2 nanowires and their catalytic properties," *Applied Catalysis B: Environmental*, vol. 180, pp. 344–350, 2016.

[20] S. Iijima, "Helical microtubules of graphitic carbon," *Nature*, vol. 354, no. 6348, pp. 56–58, 1991.

[21] Y. Zhang, N. W. Franklin, R. J. Chen, and H. Dai, "Metal coating on suspended carbon nanotubes and its implication to metal-tube interaction," *Chemical Physics Letters*, vol. 331, no. 1, pp. 35–41, 2000.

[22] Y. Tian, C. Hu, X. He, C. Cao, G. Huang, and K. Zhang, "Titania nanotube arrays for light sensor and UV photometer," *Sensors and Actuators, B: Chemical*, vol. 144, no. 1, pp. 203–207, 2010.

[23] O. K. Varghese, D. Gong, M. Paulose, K. G. Ong, and C. A. Grimes, "Hydrogen sensing using titania nanotubes," *Sensors and Actuators B: Chemical*, vol. 93, no. 1–3, pp. 338–344, 2003.

[24] C. Ruan, M. Paulose, O. K. Varghese, and C. A. Grimes, "Enhanced photo electrochemical-response in highly ordered TiO_2 nanotube-arrays anodized in boric acid containing electrolyte," *Solar Energy Materials & Solar Cells*, vol. 90, no. 9, pp. 1283–1295, 2006.

[25] M. Paulose, G. K. Mor, O. K. Varghese, S. Karthik, and A. G. Craig, "Visible light photoelectrochemical and water-photoelectrolysis properties of titania nanotube arrays," *Journal of Photochemistry & Photobiology A Chemistry*, vol. 178, no. 1, pp. 8–15, 2006.

[26] J. Gong, W. Pu, C. Yang, and J. Zhang, "A simple electrochemical oxidation method to prepare highly ordered Cr-doped titania nanotube arrays with promoted photoelectrochemical property," *Electrochimica Acta*, vol. 68, pp. 178–183, 2012.

[27] D. V. Bavykin, A. A. Lapkin, P. K. Plucinski, J. M. Friedrich, and F. C. Walsh, "Reversible storage of molecular hydrogen by sorption into multilayered TiO_2 nanotubes," *The Journal of Physical Chemistry B*, vol. 109, no. 41, pp. 19422–19427, 2005.

[28] C. S. Zhai, L. Yang, J. Wang, W. M. Zhao, and B. D. Sun, "Nanoindentation mehanical properties of Al_2O_3-3 wt% TiO_2 detonation sprayed coatings," *Journal of Aeronautical Materials*, vol. 25, no. 2, pp. 38–42, 2005.

[29] W. H. Brattain and J. Bardeen, "Surface Properties of Germanium," *Bell System Technical Journal*, vol. 32, no. 1, pp. 1–41, 1953.

[30] E. O. Johnson, "Measurement of minority carrier lifetimes with the surface photovoltage," *Journal of Applied Physics*, vol. 28, no. 11, pp. 1349–1353, 1957.

[31] A. M. Goodman, "A method for the measurement of short minority carrier diffusion lengths in semiconductors," *Journal of Applied Physics*, vol. 32, no. 12, pp. 2550–2552, 1961.

[32] L. J. Brillson, "The structure and properties of metal-semiconductor interfaces," *Surface Science Reports*, vol. 2, no. 2, pp. 123–326, 1982.

[33] Q. Zhang, D. Wang, X. Wei et al., "A study of the interface and the related electronic properties in n-Al 0.35Ga0.65N/GaN heterostructure," *Thin Solid Films*, vol. 491, no. 1-2, pp. 242–248, 2005.

[34] H. Fan, D. Wang, T. Xie, and Y. Lin, "The preparation of high photocatalytic activity nano-spindly Ag-BiVO4 and photoinduced carriers transfer properties," *Chemical Physics Letters*, vol. 640, pp. 188–193, 2015.

[35] F. Chekin, S. Bagheri, and S. B. A. Hamid, "Synthesis of Pt doped TiO_2 nanoparticles: characterization and application for electrocatalytic oxidation of L-methionine," *Sensors & Actuators B: Chemical*, vol. 177, no. 2, pp. 898–903, 2013.

[36] E. Bailón-García, F. Carrasco-Marín, F. Agustin, A. Pérez-Cadenas, and F. J. Maldonado-Hóda, "Influence of the pretreatment conditions on the development and performance of active sites of Pt/TiO_2 catalysts used for the selective citral hydrogenation," *Journal of Catalysis*, vol. 327, pp. 86–95, 2015.

[37] J. L. Li, W. Z. Chen, B. Wu et al., "Synthesis and characterization of Ag-doped TiO_2 nanotubes," *Journal of Functional Materials*, vol. 40, no. 8, pp. 953–957, 2012.

[38] X. Zhu, M. Shen, L. L. Lobban, and R. G. Mallinson, "Structural effects of Na promotion for high water gas shift activity on Pt-Na/TiO2," *Journal of Catalysis*, vol. 278, no. 1, pp. 123–132, 2011.

[39] H. Zhu, D. H. Anjum, Q. Wang et al., "Sn surface-enriched Pt-Sn bimetallic nanoparticles as a selective and stable catalyst for propane dehydrogenation," *Journal of Catalysis*, vol. 320, no. 1, pp. 52–62, 2014.

[40] R. K. Sahu, D. Mukherjee, J. P. Tiwari, T. Mishra, S. K. Roy, and L. C. Pathak, "Influence of foreign Fe ions on wet chemical synthesis of Pt nanoparticle thin films at ambient temperature: In situversus direct addition," *Journal of Materials Chemistry*, vol. 19, no. 37, pp. 6810–6815, 2009.

[41] J. L. Li, W. Z. Chen, J. J. Bi, D. J. Guo, B. C. Yang, and Z. W. Zhou, "Synthesis of Ag-TiO_2 Nanotubes in ambient atmosphere and kinetics of photocatalytic reaction," *Chinese Journal of Sensors Actuators*, vol. 23, no. 5, pp. 617–620, 2010.

[42] Z. Zhao, C.-T. Poon, W.-K. Wong et al., "Synthesis, photophysical characterization, and surface photovoltage spectra of windmill-shaped phthalocyanine-porphyrin heterodimers and heteropentamers," *European Journal of Inorganic Chemistry*, no. 1, pp. 119–128, 2008.

[43] L. Kronik and Y. Shapira, "Surface photovoltage phenomena: Theory, experiment, and applications," *Surface Science Reports*, vol. 37, no. 1, pp. 1–206, 1999.

[44] M. Jakob, H. Levanon, and P. V. Kamat, "Charge distribution between UV-irradiated TiO_2 and gold nanoparticles: determination of shift in the Fermi level," *Nano Letters*, vol. 3, no. 3, pp. 353–358, 2003.

[45] Z. H. Li, D. J. Wang, P. Wang, X. Wei, and Q. L. Zhang, "Research on characteristics of photogenerated charge in nano-TiO_2," *Acta Physico-Chimica Sinica*, vol. 21, no. 3, pp. 310–314, 2005.

[46] M. H. William, *Handbook on Chemistry and Physics*, CRC, Florida, Fla, USA, 2008.

[47] A. Hagfeldtt and M. Gratzel, "Light-induced redox reactiongs in nanocrystalline systems," *Chemical Reviews*, vol. 95, pp. 49–68, 1995.

[48] A. L. Linsebigler, G. Q. Lu, and J. T. Yates Jr., "Photocatalysis on TiO_2 surfaces: principles, mechanisms, and selected results," *Chemical Reviews*, vol. 95, no. 3, pp. 735–758, 1995.

[49] X. Zhang, Y. Lin, D. He, J. Zhang, Z. Fan, and T. Xie, "Interface junction at anatase/rutile in mixed-phase TiO2: Formation and photo-generated charge carriers properties," *Chemical Physics Letters*, vol. 504, no. 1-3, pp. 71–75, 2011.